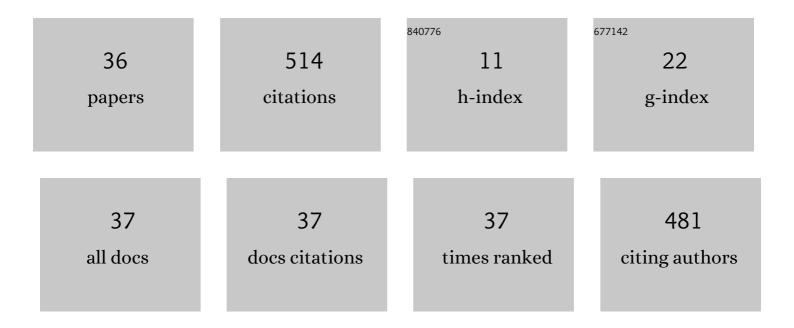
## Hiroya Abe

List of Publications by Year in descending order

Source: https://exaly.com/author-pdf/6629004/publications.pdf Version: 2024-02-01



HIDOVA ARE

#	Article	IF	CITATIONS
1	Transdermal electroosmotic flow generated by a porous microneedle array patch. Nature Communications, 2021, 12, 658.	12.8	134
2	Electrochemical Imaging of Dopamine Release from Three-Dimensional-Cultured PC12 Cells Using Large-Scale Integration-Based Amperometric Sensors. Analytical Chemistry, 2015, 87, 6364-6370.	6.5	63
3	Electrochemicolor Imaging Using an LSI-Based Device for Multiplexed Cell Assays. Analytical Chemistry, 2017, 89, 12778-12786.	6.5	34
4	Fe azaphthalocyanine unimolecular layers (Fe AzULs) on carbon nanotubes for realizing highly active oxygen reduction reaction (ORR) catalytic electrodes. NPG Asia Materials, 2019, 11, .	7.9	30
5	Potentiometric bioimaging with a large-scale integration (LSI)-based electrochemical device for detection of enzyme activity. Biosensors and Bioelectronics, 2016, 77, 709-714.	10.1	21
6	Reversible Shape Transformation of Ultrathin Polydopamine-Stabilized Droplet. Langmuir, 2017, 33, 6404-6409.	3.5	21
7	Bioimaging using bipolar electrochemical microscopy with improved spatial resolution. Analyst, The, 2020, 145, 6895-6900.	3.5	20
8	Chemical Imaging Using a Closed Bipolar Electrode Array. Chemistry Letters, 2018, 47, 843-845.	1.3	19
9	Feedback mode-based electrochemical imaging of conductivity and topography for large substrate surfaces using an LSI-based amperometric chip device with 400 sensors. Journal of Electroanalytical Chemistry, 2015, 741, 109-113.	3.8	17
10	Electrochemical Imaging for Single-cell Analysis of Cell Adhesion Using a Collagen-coated Large-scale Integration (LSI)-based Amperometric Device. Electrochemistry, 2016, 84, 364-367.	1.4	14
11	Biomimetic Bubble-Repellent Tubes: Microdimple Arrays Enhance Repellency of Bubbles Inside of Tubes. Langmuir, 2017, 33, 585-590.	3.5	12
12	Preparation of Hierarchic Porous Films of α-MnO <sub>2</sub> Nanoparticles by Using the Breath Figure Technique and Application for Hybrid Capacitor Electrodes. ACS Omega, 2019, 4, 3827-3831.	3.5	12
13	N- and Fe-containing Carbon Films Prepared by Calcination of Polydopamine Composites Self-assembled at Air/Water Interface for Oxygen Reduction Reaction. Chemistry Letters, 2019, 48, 102-105.	1.3	12
14	S/N Co-Doped Hollow Carbon Particles for Oxygen Reduction Electrocatalysts Prepared by Spontaneous Polymerization at Oil–Water Interfaces. ACS Omega, 2020, 5, 18391-18396.	3.5	12
15	Biodegradable Porous Microneedles for an Electric Skin Patch. Macromolecular Materials and Engineering, 2021, 306, 2100171.	3.6	11
16	Porous Microneedle Patch for Electroosmosisâ€Promoted Transdermal Delivery of Drugs and Vaccines. Advanced NanoBiomed Research, 2022, 2, 2100066.	3.6	11
17	Thermally Stable Honeycombâ€Patterned Porous Films of a Poly(L″actic acid) and Poly(D″actic acid) Stereo Complex Prepared Using the Breath Figure Technique. Macromolecular Materials and Engineering, 2016, 301, 523-529.	3.6	9
18	Totally transparent hydrogel-based subdural electrode with patterned salt bridge. Biomedical Microdevices, 2020, 22, 57.	2.8	9

Hiroya Abe

#	Article	IF	CITATIONS
19	Bio-inspired Incrustation Interfacial Polymerization of Dopamine and Cross-linking with Gelatin toward Robust, Biodegradable Three-Dimensional Hydrogels. Langmuir, 2021, 37, 6201-6207.	3.5	9
20	Aqueous dispersion and tuning surface charges of polytetrafluoroethylene particles by bioinspired polydopamine–polyethyleneimine coating via one-step method. Royal Society Open Science, 2021, 8, 210582.	2.4	9
21	Biomimetic antibiofouling oil infused honeycomb films fabricated using breath figures. Polymer Journal, 2021, 53, 713-717.	2.7	8
22	Redox cycling-based electrochemical CMOS imaging sensor for real time and selective imaging of redox analytes. Sensors and Actuators B: Chemical, 2020, 304, 127245.	7.8	7
23	Totally organic electrical skin patch powered by flexible biobattery. JPhys Energy, 2020, 2, 044004.	5.3	7
24	Simultaneous and Selective Imaging of Dopamine and Glutamate Using an Enzymeâ€modified Largeâ€scale Integration (LSI)â€based Amperometric Electrochemical Device. Electroanalysis, 2018, 30, 2841-2846.	2.9	6
25	Light in Electrochemistry. Electrochem, 2021, 2, 472-489.	3.3	3
26	Synthesis of unused-wood-derived C-Fe-N catalysts for oxygen reduction reaction by heteroatom doping during hydrothermal carbonization and subsequent carbonization in nitrogen atmosphere. Philosophical Transactions Series A, Mathematical, Physical, and Engineering Sciences, 2021, 379, 20200348.	3.4	3
27	Shape Transformation Photolithography: Self-Assembled Arrays of Suspended MEMS Structures from Patterned Polymer Membranes. ACS Omega, 2018, 3, 18489-18498.	3.5	1
28	The Development of the Technique for Physical Bonding between Gel/Silicone for the Hydrogel Salt Bridge Electrode. ECS Meeting Abstracts, 2020, MA2020-02, 3650-3650.	0.0	0
29	Biodegradable Porous Microneedle for Electric Skin Patch. ECS Meeting Abstracts, 2020, MA2020-02, 3288-3288.	0.0	0
30	Wearable Patch-Type Transepidermal Potential Measurement Device with Porous Microneedle. ECS Meeting Abstracts, 2020, MA2020-02, 3651-3651.	0.0	0
31	Development of Low Power Consumption Electrochromic Device Using Spontaneous Discoloration Reaction. ECS Meeting Abstracts, 2020, MA2020-02, 3576-3576.	0.0	0
32	Hydrogel-Based Transparent Subdural Electrode with Salt Bridge As Interface to Brain Surface. ECS Meeting Abstracts, 2020, MA2020-02, 2793-2793.	0.0	0
33	Development of Permeable and Transparent Intracranial Electrode Embedded in Hydrogel Substrate. ECS Meeting Abstracts, 2020, MA2020-02, 3311-3311.	0.0	0
34	The Optimized Fabrication of a Polymeric Porous Microneedle for Effective Iontophoresis. ECS Meeting Abstracts, 2020, MA2020-02, 3649-3649.	0.0	0
35	Designed Electroosmotic Polymer for an Anti-Drying Contact Lens Device. ECS Meeting Abstracts, 2020, MA2020-02, 3300-3300.	0.0	0
36	Tough Mechanically Interlocked Transparent Interface of Hydrogel and Elastomer for Biomedical Applications. Macromolecular Materials and Engineering, 0, , 2100931.	3.6	0